Impact Characterization of a Carbon Fiber-Epoxy Laminate Using a Nonconservative Model

A. B. Martínez, M. Sánchez-Soto, J. I. Velasco, M. Ll. Maspoch, O. O. Santana, A. Gordillo

Centre Català del Plàstic. Universitat Politécnica de Catalunya C/Colom n° 114 08222 Terrassa, Spain

Received 21 January 2005; accepted 8 March 2005
DOI 10.1002/app.21894
Published online in Wiley InterScience (www.interscience.wiley.com).

ABSTRACT: The study of polymer and composite behavior under high strain rates is of fundamental relevance to determine the material suitability for a selected application. However, the impact phenomenon is a very complicated event, mainly due to the short duration, large deformation, and high stresses developed in the sample. In this work, we have performed impact tests over a carbon fiber reinforced epoxy using low-energy in the striker. A nonconservative and nonlineal spring-dashpot series model has been proposed to reproduce the material behavior. The model considers simultaneously both flexural and indentation phenomena accounting for energy losses by means of the restitution coefficient. Using this model, an excellent fit between the predicted and the experimental force-time trace has been obtained below the composite failure point, which was recognized by a separation of both mentioned curves. As the epoxy-fiber laminate has a very low viscoelasticity, the high strain rate Young's modulus obtained from the model was compared with that extracted from a conventional three point bending test, finding a very good match between the values. The study of the dashpot coefficients allows concluding that the dominant mechanism is the composite flexion, while the indentation effects contribution takes on importance at low impact velocities. © 2005 Wiley Periodicals, Inc. J Appl Polym Sci 97: 2256–2263, 2005

Key words: composites; impact resistance; low-energy impact; modeling; restitution coefficient

INTRODUCTION

Materials based on an epoxy matrix reinforced with carbon fibers due to its excellent properties, such as high specific strength and stiffness or high fatigue and corrosion resistance, form one of the composite families with broad technological applications. Nevertheless, fiber reinforced composite laminates are susceptible to being damaged if subjected to low-energy impact loading. This type of loading could arise from the manufacturing process or as a consequence of the service life, but a common trend in both situations is its subcritical failure character. Typical examples of low-energy impact events in aeronautics can be caused by birds, debris during take-off or landing, falling utensils, and so forth. The damage caused by these impacts can be manifested as a combination of matrix cracking, interply delamination, detaching at the fiber-matrix interface, or fiber fracture,[1] all of them origins of crack growth. The presence of cracks can alter the composite mechanical properties, leading to an earlier failure; thus, this is one of the key factors limiting composite structures' service life.

Correspondence to: M. Sánchez-Soto (m.sanchez-soto@upc.edu).

Journal of Applied Polymer Science, Vol. 97, 2256–2263 (2005)

The low-energy impact response of fiber-reinforced composites has been a subject of intense research efforts using many different approaches and technical procedures.[2–4] The greatest part of this research is focused in the damage originated after an out-of-plane impact loading, as this is one of the mechanically weakest directions in the composite. The instrumented falling weight impact (IFWI) is one of the methods used to study transverse impact behavior on solids. In this procedure, a mass is dropped from a determined height to have an impact on the sample with the aim of measuring its response. The striker has a load sensor located very close to the impact point, so it is possible to record the whole impact event extracting force-time or force-displacement evolutions. From these records, some of the sample mechanical properties can be extracted.[3,5] In addition, the damage caused on the specimen could be modified by introducing a slight variation on the striker energy; as a result, the technique is useful to investigate situations like when internal damage is created by a low impact.

Under a low-velocity impact loading, the laminate behavior could be separated in two parts; the localized contact with the falling tup and the following flexural deflection. The contact between laminate and tup results in an instantaneous pressure over the compressed area, which in turn originates a local deformation over the composite surface. Indentation, that is, the dent depth resulting from the contact between

the target surface and the incident object, may be modeled, taking into account the Hertz contact law.[6] The Hertz law, originally developed for static conditions, is used in impact situations if the contact time is large in comparison with the period of system oscillations, as occurs in this case. After the indentation, the laminate behavior can be analyzed with the theory of deflection for flat plates.[7]

The different approaches performed to predict the materials' impact behavior have been traditionally based on conservative mass-spring models.[8,9] Normally these models assume an ideal linear elastic material behavior, neglecting the energy losses arising from the impact event. The obtained results, in spite of their good approach, do not exactly represent the behavior of polymeric composites because many energy dissipation mechanisms are involved when dealing with this kind of material. Some of the proposed models include flexion[9] or indentation[10] in separate ways, although some simultaneous but conservative models have been proposed.[11] Wu and Yu[12] applied two nonlinear springs with strain dependence to represent the flexural and superficial deformation; however, as the test was carried out over aluminum samples, indentation effects were not considered. Akil and Cantwell[13] have used a simple energy-balance similar to the one outlined by Abrate[14] to predict the maximum force developed impacting foam-based sandwich structures. Usually the description of the impact behavior considers the most important contribution, indentation or flexion, neglecting the other one. However, a complete fitting model should take into account simultaneously sample flexion as well as indentation. In a recent work, an approach to the impact behavior of glassy thermoplastic polystyrene composites has been carried out using a nonconservative flexural model with an analytical solution,[15] but no indentation effects were considered. In this work we have utilized a similar system to the one previously mentioned, but including the necessary elements to reproduce indentation.

During the impact event, the originated energy losses came from different contributions: The viscoelastic nature of the sample, the friction between striker and sample, sample vibration and stress waves, and, finally, specimen plastic deformation. The dissipation of kinetic energy through vibration and stress waves is negligible, the latter being about 3% of the initial energy.[16] The impact energy losses were considered, here introducing into the model the restitution coefficient (ε). The restitution coefficient is an empirical parameter used to deal with the loss of energy on impact and is defined as the ratio between the approach velocity and the velocity after the collision. The coefficient has ever a positive value, being the limit one for a pure elastic contact and zero for a pure inelastic contact.[17]

TABLE I
Main Composite Characteristics

Property	Property values
Superficial weight (g/cm^2)	193 ± 8
Density (g/cm^3)	1.78 ± 0.05
Filament shape	Circular
Tow cross-section (mm^2)	0.12
Young's tensile modulus 0° (GPa)	67.73
Young's tensile modulus 90° (GPa)	65.5
Young's compression modulus 0° (GPa)	60.1
Maximum tensile stress 0° (MPa)	829.4
Maximum tensile stress 90° (MPa)	794.8
Maximum compression stress 0° (MPa)	884.7

This work has been carried out with several purposes. The first one is to determine the feasibility of the low-energy impact technique to the mechanical characterization of a fiber-reinforced composite. The second objective is the experimental determination of impact energy losses through the restitution coefficient. The last objective is to validate the proposed nonconservative model, including on it the indentation effects by its application to the composite, contrasting the theoretical and experimental impact response.

EXPERIMENTAL

Hexcel Corp. (Parla, Spain) supplied the composites in the form of rectangular panels. The composites were formed mixing carbon fiber and an epoxy matrix. The carbon fiber, whose commercial name is Magnamite AS4, is based on polyacrylonitrile having the fibers disposed in 3000 filament count tows; the fiber was superficially treated to improve its interlaminar shear properties. The employed matrix was of epoxy type having a dry Tg of 195°C. The resin curing process was done at 180°C during 2 h. The laminate was formed using a plain woven fabric with the fibers disposed in a regular pattern at 0/90°. The composite fiber area weight was 193 g/m^2, and its density was 1.78 g/cm^3. The relation matrix to fiber was 40/60 in weight.

The main laminate properties are depicted in Table I. From the panels, square specimens 83 mm in width and 2.59 mm thickness were cut with a diamond saw. The samples were then placed simply supported on an annular ring with inner and outer diameters of 60 mm and 80 mm, respectively.

Falling weight impacts were carried out with a Ceast Dartvis (Torino, Italy) instrumented with load gauges. The hemispherical dart headstock had a diameter of 12.7 mm, and the data acquisition frequency was set to the maximum of 125 kHz to obtain the largest number of experimental points. The striker mass was kept constant and equal to 0.7437 kg; while

the impact velocity, and thus the energy, was modified, changing the drop height between the limits of 0.5 m/s and 2.5 m/s In all cases, the experiments were carried out at room temperature.

Previous to the impact testing, a careful velocity calibration was performed. A photoelectrical cell was located very close to the impact point in order to obtain the true velocity just at the impact moment. This experimental velocity was then compared with the theoretical one derived from the drop height. The drop heights were varied from 13 mm to 275 mm, and the experiences were replicated three times, making a total of 400 essays. Under 13 mm of height drop, the frictional effects were important and the photoelectric measurements had a lack of precision; for these reasons, impacts fewer than 13 mm heights were discarded.

MODEL DESCRIPTION

Restitution coefficient

The determination of the restitution coefficient needs knowledge of the striker velocity just before and after the impact. If v_0 is the velocity of the striker just before the collision and v_1 is the velocity just after contact, both expressed in m/s, the restitution coefficient can be found by:

$$\varepsilon = \frac{v_1}{v_0} \tag{1}$$

After calibration, v_0 was obtained applying the equation:

$$v_0 = 0.9686\sqrt{2gh} \tag{2}$$

where g (m/s^2) is the gravitational acceleration and h (m) is the height of drop.

The v_1 value can also be extracted equating impulse and momentum; the expression results then in:

$$d(m\dot{x}) = -F(t)\,dt \tag{3}$$

where m is the falling mass (kg), $\dot{x}$ is the velocity (m/s), F in Newtons is the recorded force, and t is the time expressed in seconds. If this expression is integrated between the initial impact moment where $t = 0$ and $\dot{x} = v_0$, up to the final impact moment where $t = tc$ and $\dot{x} = v_1$, tc is the time while striker and sample remain in contact, and we arrive at the following expression:

$$\int_{v_0}^{v_1} mv = \int_0^{t_c} F(t)\,dt \tag{4}$$

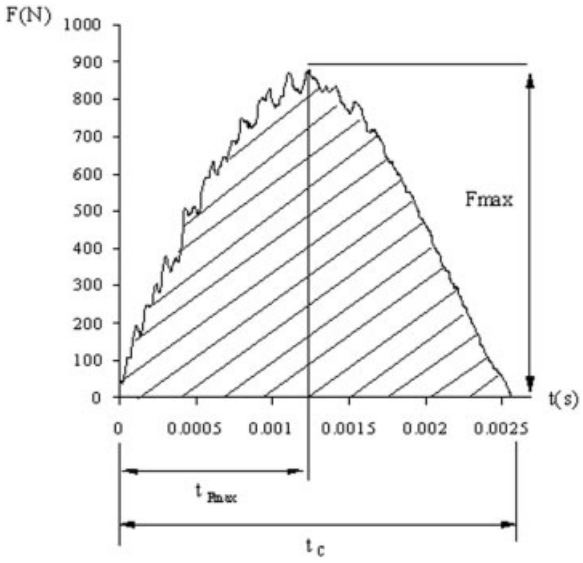

Figure 1 Experimental force-time curve at 60 mm height, showing the principal experimental variables.

Introducing in the above expression the restitution coefficient [eq. (1)], we find:

$$\varepsilon = \frac{\int_0^{t_c} F\,dt}{mv_0} - 1 \tag{5}$$

The upper term of the above expression can be calculated by integration of the experimental recorded force-time trace. In Figure 1, a typical impact curve is represented. In this picture the area enclosed by the curve represents the integral term.

Flexural and indentation nonconservative model

To explain the complete laminate behavior, the proposed model is represented by the conjunction of two systems, one representing flexion and the other representing indentation. In both cases, all energetic losses are joined and considered in only one element, mechanically represented by a dashpot, as shown in Figure 2. The part representing flexion is followed by a similar configuration of spring-dashpots in series to represent indentation; however, in this latter case, the spring constant is nonlinear. In Figure 2, m is the falling mass, K the spring constant, and C the damping constant. The sub index i is used to denote indentation while f means flexion. As a consequence of the very small specimen deflections, the effect of the gravity term is discarded.

If we express the equations representing the model, it can be appreciated that the applied force is the same for all the single elements, and the total displacement is the sum of each single displacement. The describing equations are as follows:

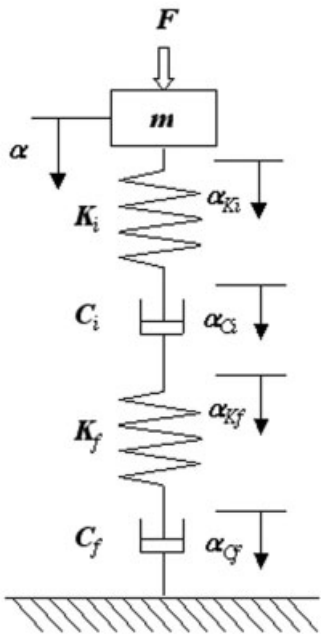

Figure 2 Sketch of the complete model (indentation + flexion) showing the four series elements and the respective constants and variables.

$$F_m = m\ddot{\alpha} \tag{6}$$

$$F_{Ci} = C_i \dot{a}_{Ci} \tag{7}$$

$$F_{Cf} = C_f \dot{\alpha}_{Cf} \tag{8}$$

$$F_{Kf} = K_f \alpha_{kf} \tag{9}$$

$$F_{Ki} = K_i \alpha_{ki}^{3/2} \tag{10}$$

where eq. (10) expresses the Hertz law for contact and the displacements represented by the symbol α are measured in m.

The constants K_f (N/m) and K_i (N/m$^{3/2}$) are derived from the simply supported deflection of a flat plate loaded in its center,[7] and from the application of the contact law to the particular case of a sphere and half-space target.

$$K_f = \frac{16\pi(1+\upsilon_2)D}{(3+\upsilon_2)r^2} = \frac{4\pi E e^3}{3(3+\upsilon_2)(1-\upsilon_2)r^2} \tag{11}$$

$$K_i = \frac{4\sqrt{R}}{3\pi}\left(\frac{1-\upsilon_1^2}{E_1} + \frac{1-\upsilon_2^2}{E_2}\right)^{-1} \tag{12}$$

where D (Nm) is the sample compliance; r (m), the support radius; R (m), the tup radius; E (N/m^2), the Young's modulus; e (m), the specimen thickness; υ, the Poisson coefficient; and the subscripts 1 and 2 represent striker and target, respectively.

The flexural dashpot constant can be obtained from the expression of a nonconservative spring-dashpot series model for flexion:[18]

$$\zeta = \frac{\sqrt{K_f m}}{2C_f} = \sqrt{\frac{1}{1+\left(\frac{\pi}{\ln \varepsilon}\right)^2}} \tag{13}$$

As a result, C_f (Kg/s) is:

$$C_f = \frac{\sqrt{K_f m\left(1+\left(\frac{\pi}{\ln \varepsilon}\right)^2\right)}}{2} \tag{14}$$

The expression for Ci (Kg/s) has to be adjusted, but with the restriction that the whole system solution has to fulfill the expression of the restitution coefficient [eq. (5)].

Due to the serial arrangement of the model, the force applied over the system is the same as that applied over each element. Since the dashpots are linear, both can be joined to form an equivalent one (Fig. 3), and then:

$$\frac{F_{Ceq}}{C_{eq}} = \frac{F_f}{C_f} + \frac{F_i}{C_i} \tag{15}$$

and finally we arrive at an expression for the coupled dashpot constant:

$$\frac{1}{C_{eq}} = \frac{1}{C_f} + \frac{1}{C_i} \tag{16}$$

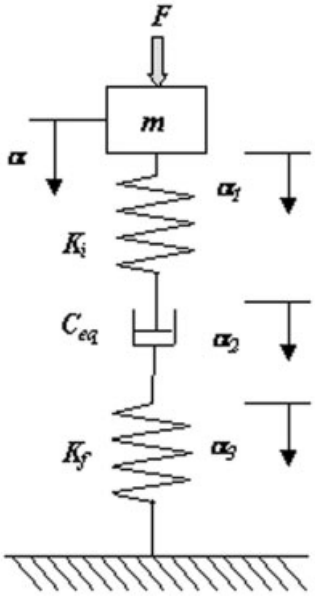

Figure 3 Equivalent model with indentation and flexural dashpots joined in an equivalent one.

or equivalently:

$$C_{eq} = \frac{1}{\frac{1}{C_f} + \frac{1}{C_i}} \tag{17}$$

From Figure 3, it results also:

$$F_{Ceq} = C_{eq}\dot{\alpha}_2 \tag{18}$$

The dashpot simplification cannot be applied to the springs, because the spring indentation element is nonlinear. The equations for the model are then:

$$\alpha_{Ki} = \alpha_1 \tag{19}$$

$$\alpha_{Ci} + \alpha_{Cf} = \alpha_2 \tag{20}$$

$$\alpha_{Kf} = \alpha_3 \tag{21}$$

Once the expressions for the dashpot and spring constants have been analyzed, we can express the differential equation describing the system behavior in the following form:

$$F = m\ddot{\alpha} = K_f\alpha_1 = C_{eq}\dot{\alpha}_2 = K_i\alpha_3^{3/2} \tag{22}$$

$$\alpha = \alpha_1 + \alpha_2 + \alpha_3 \tag{23}$$

To reduce variables, from the two above expressions it is possible to obtain:

$$\ddot{\alpha} = \frac{K_f}{m}\,\alpha_1 \tag{24}$$

$$\alpha_3 = \left[\frac{C_{eq}}{K_i}\,\dot{\alpha}_2\right]^{2/3} \tag{25}$$

$$\alpha_1 = \alpha - \alpha_2 - \alpha_3 \tag{26}$$

Properly combining the three preceding equations yields:

$$\ddot{\alpha} = \frac{K_f}{m}\left(\alpha - \alpha_2 - \left[\frac{C_{eq}}{K_i}\,\dot{\alpha}_2\right]^{2/3}\right) \tag{27}$$

and from equation 22, we find:

$$\dot{\alpha}_2 = \frac{K_f}{C_{eq}}\,\alpha_1 \tag{28}$$

$$\dot{\alpha}_2 = \frac{K_f}{C_{eq}}\left(\alpha - \alpha_2 - \left[\frac{C_{eq}}{K_i}\,\dot{\alpha}_2\right]^{2/3}\right) \tag{29}$$

Equations 28 and 29 reflect the system behavior; however, the system equation does not have an analytical solution. Because of this, it is necessary to find a numerical function that allows solving the problem.

Numerical resolution

The numerical resolution applied is based upon iterative algorithms taking as reference an initial well-known point. The convenience of the application of one or the other procedure depends on the studied range and the required precision. In the present case, the interval range where the solution has to be found is quite large; then, easier iterative methods such as Euler or Euler-Gauss will render nonvalid solutions far away from the initial point. Because of this, the fourth order Runge–Kutta method was selected. This method is based on the calculation of the slope between the known and unknown points. Its implementation could be performed using a normal computer spreadsheet.

To solve the differential equation it is useful to express the equations in the same manner. Equations 28 and 29 are two of the needed functions, but we need two more equations to find the solutions: $\alpha,\dot{\alpha},\alpha_2$ and $\dot{\alpha}_2$. We can express:

$$\dot{\alpha}_2 = \frac{d\alpha_2}{dt} \tag{30}$$

To obtain $\dot{\alpha}_2$ it would be necessary to set an expression relating the equivalent dashpot strain rate with the other system variables. Although this procedure is possible, it derives in a set of noncommon differential equations, complicating the resolution. Instead, at the impact origin, the value of $\dot{\alpha}_2$ is null, so we can use the following approach:

$$\dot{\alpha}_2 = \frac{d\alpha_2}{dt} = \frac{\alpha_{2(i)} - \alpha_{2(i-1)}}{\Delta t} = \frac{\Delta\alpha_2}{\Delta t} \tag{31}$$

As a result, the following group of equations describes the system behavior:

$$f_1 = \dot{\alpha} \tag{32}$$

$$f_2 = \frac{K_f}{m}\left(\alpha - \alpha_2 - \left[\frac{C_{eq}}{K_i}\,\dot{\alpha}_2\right]^{2/3}\right) \tag{33}$$

$$f_3 = \frac{K_f}{C_{eq}}\left(\alpha - \alpha_2 - \left[\frac{C_{eq}}{K_i}\,\dot{\alpha}_2\right]^{2/3}\right) \tag{34}$$

$$\dot{\alpha}_2 = \frac{\Delta\alpha_2}{\Delta t} \tag{35}$$

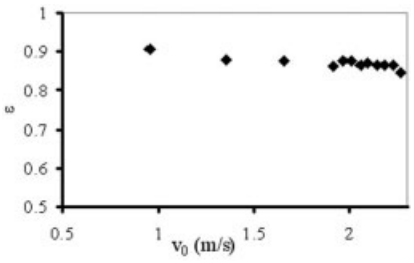

Figure 4 Evolution of the composite restitution coefficient versus the measured velocity.

The method was programmed with a 1.5×10^{-6} s time interval. The system boundary conditions were taken as follows: At the initial moment, the velocity is equal to that measured by the photoelectrical cell, then $\dot{\alpha}_{t=0} = V_0$, and the initial positions of all elements are: ($\alpha = \alpha_1 = \alpha_2 = \alpha_3 = 0$). The model parameters are the striker falling mass (m), and the spring and dashpot constants (K_i, K_f, and C_{eq}). The adjusting parameter C_i is obtained after a finite number of iterations imposing the condition that the restitution coefficient of the numerical curve matches the experimental value (eq. (5) and Fig. 1).

RESULTS AND DISCUSSION

Restitution coefficient

The representation of the composite restitution coefficient is displayed in Figure 4. It can be observed that the restitution coefficient varies from a maximum of ~ 0.9 to a minimum around 0.85. This circumstance implies that even in a very low impact speed event, there is a loss of the striker energy absorbed mainly by the specimen. The variation of the laminate restitution coefficient with the drop velocity is very low. This result is reasonable if we take into account the low viscoelasticity of the tested laminate. Further, the energy losses are velocity dependent, with a slight decrease in the ε value.

The experimental values of the restitution coefficient, lower than 1, confirm that the employment of fully conservative models is not appropriate. On the other hand, it is corroborated that the restitution coefficient depends on the testing conditions.

Model application

Figure 5 shows the representation of the experimental impact graphs coupled with the curves derived from the model application. The experimental curves show some dynamic effects. These oscillations, superimposed in the graphs, are a consequence of the slight gap between the impact point and the load gauge location; but, as can be appreciated, its magnitude is very low in comparison with the force range. Obviously, the calculated curves show no oscillations; however, in spite of these differences, a very good match between real and calculated graphs is observed.

The correlation between the experimental and calculated traces is maintained while the specimen compliance does not change. In the laminate case, this is accomplished up to a 280mm height drop, or equivalently up to an impact energy of 2.038 J. If the impact energy is raised, composite failure is detected in the response curve by a separation between the theoretical and the experimental curves, as shown in Figure 6. It can also be observed that the experimental curve changes from a round shape to a sharp trace with a peak followed by broad oscillations. This kind of curve is typically observed in specimens that undergo a splitting break after impact; however, in our experience, no signs of external damages or dents were observed in the composites. Thus, the change in the composite compliance must be a consequence of the appearance of internal damage, probably in the form of delamination or fiber matrix detaching. The method proposed could be useful to detect the energy onset to create the first sample damage. If the evolution of the recorded force is plotted versus the impact velocity, in the resulting graph a change in the slope of the adjusting lines can be observed. The point where the slope changes defines the onset of damage, as can be appreciated from Figure 7.

In a complementary way, a study of the dashpot constants evolution (C_{eq}, C_i, C_f) versus the impact velocity [Fig. 8(a)] and the restitution coefficient [Fig. 8(b)] was carried out. The increment of the impact

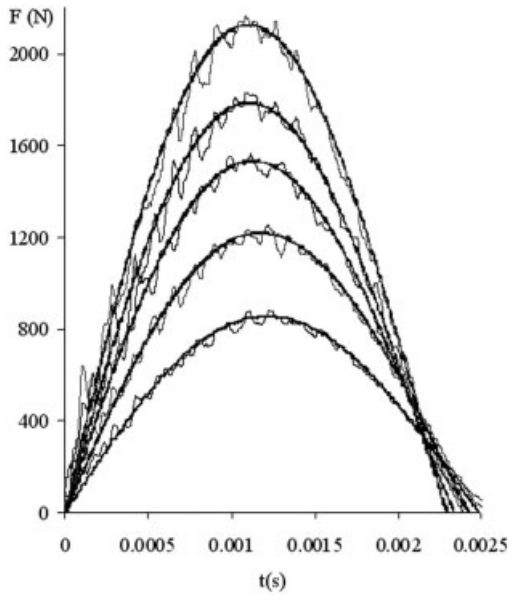

Figure 5 Representation of experimental and calculated curves. Drop heights from bottom to top are: 50mm, 100 mm, 150 mm, 200 mm, and 280 mm.

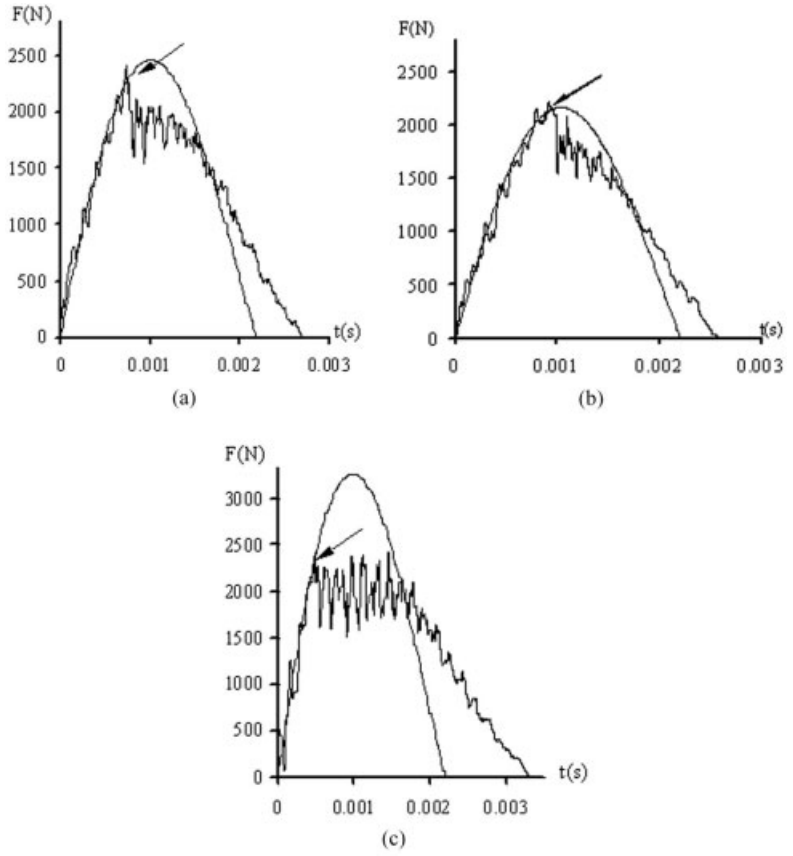

Figure 6 Detection of failure point by separation between the theoretical and the experimental curves. The onset of damage is indicated by the arrows. Drop heights are as follows: (a) h = 300 mm, (b) h = 400 mm, and (c) h = 800 mm. The model impact curve is represented by a continuous line.

speed, or equivalently the decrease of the restitution coefficient, yields a lower value of the equivalent dashpot coefficient. The equivalent coefficient accounts for losses due to flexural and indentation phenomena and, in accordance with eq. (17), the decrement of this coefficient implies an increment of the flexural or indentation coefficient. The evolution of C_f versus the velocity is almost constant whatever the velocity value; on the other hand, its medium value is

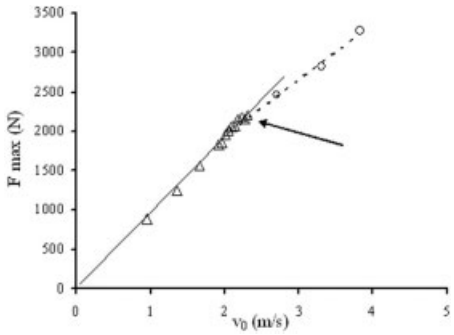

Figure 7 Plot of the recorded experimental force versus the measured impact velocity. The arrow indicates the point at which damage initiates in the composite.

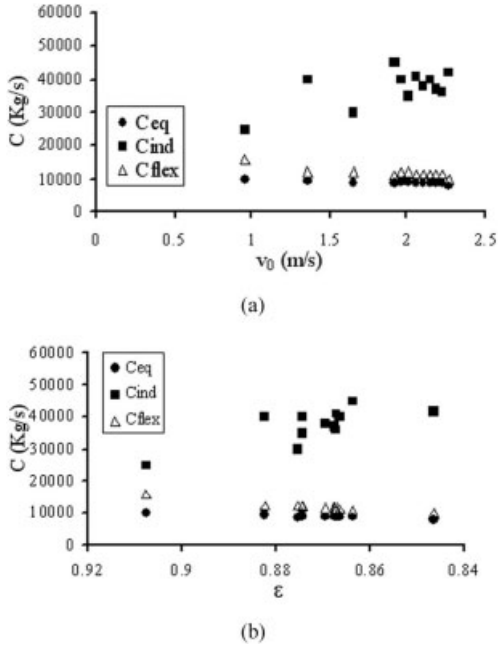

Figure 8 Representation of the dashpot constants: (a) evolution versus the measured impact velocity, and (b) evolution versus the restitution coefficient.

approximately four times lower than C_i. As a result, the larger part of the energy losses (ca. 80%) can be attributed to flexural phenomena while the rest is attributed to indentation effects.

From the proposed model and applying the flexural equations of a simply supported plate, it is possible to obtain the composite Young's modulus. Its evolution is depicted in Figure 9 versus the measured impact velocity. In the range of velocities studied, the composite Young's modulus was, as expected, almost constant as a result of the low material viscoelasticity. To have an independent way to verify the accuracy of the high-velocity modulus extracted from the model, the composite was tested in a three point bending arrangement at a very low velocity of 1mm/min. The results of this comparison are included in Table II. The obtained values agree well, with the difference between both measurements lower than 1%. This fact confirms that the proposed model is useful to determine the Young's modulus of the samples tested under high-velocity conditions.

TABLE II
Comparison of the Composite Young's Modulus in Flexion under Low and High-Velocity Testing Conditions. (The results are the mean of 7 samples at low velocity and 20 specimens at high velocity.)

Specimen thickness (mm)	Low-velocity (1 mm/min)	High-velocity (2 m/s)
	E flexural (MPa)	*E* model (MPa)
2.59 ± 0.02	39983 ± 1670	39596 ± 1329

CONCLUSIONS

Even performing low-velocity impacts, energy losses are significant. In the case of the carbon fiber-epoxy laminate, although it has low viscoelasticity, the restitution coefficient was found to be near 0.85, meaning that the conservative model approach cannot fully represent the material impact behavior. On the other hand, the nonconservative complete series model represents a good approach to the experimental results because it considers both flexural and indentation effects.

The model allows determining the high strain rate Young's modulus. In the epoxy reinforced carbon fiber laminate, the evolution of the Young's modulus with the impact velocity is constant over the whole testing range, a fact consistent with the low composite viscoelasticity. The comparison between theoretical and experimental curves yields the energy and maximum force necessary to produce the first damage on the tested material.

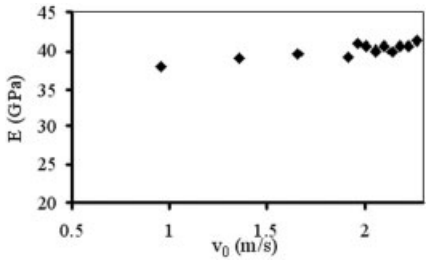

Figure 9 Composite Young's modulus evolution versus the impact velocity.

The authors thank the Ministerio de Ciencia y Tecnología (Spain) for financial support given through project MAT-2000–1112, and Hexcel Corp. for kindly supplying the composites.

References

1. Abrate, S. Appl Mech Rev 1991, 44, 155.
2. Sohn, M. S.; Hu, X. K.; Kim, J. K.; Walter, L. Compos B 2000, 31, 681.
3. Naik, N. K.; Ramasimha, R.; Arya, H.; Prabhu, S. V.; ShamaRao, N. Compos B 2001, 32, 565.
4. Caprino, G.; Langella, A.; Lopresto, V. Compos B 2003, 34, 319.
5. Pavan, A. In: Fracture Mechanics Testing Methods for Polymers Adhesives and Composites, ESIS Publication 28; Moore, D. R.; Pavan, A.; Williams, J. G., Eds.; Elsevier Science: Amsterdam, 2001; pp 27–58.
6. Sun, C. T.; Dicken, A.; Wu, H. F. Compos Sci Technol 1993, 49, 139.
7. Timoshenko, S. P.; Woinowsky-Krieger, S. Theory of Plates and Shells; Mc Graw-Hill: Kogakusha, Tokyo, 1984; 2nd ed.
8. Grezckuck, L. B. In: Impact Dynamics. Ed.; John Wiley & Sons: New York, 1982.
9. Casiraghi, T.; Castiglioni, G.; Ronchetti, T. J Mater Sci; Bitacora Publicidad: Gijon, Spain, 1988, 23, 459.
10. Sburlati, R. Compos B 2002, 33, 325.
11. Pang, S. S.; Zhao, Y. Polym Eng Sci 1991, 31, 1461.
12. Wu, K. Q.; Yu, T. X. Int J Impact Eng 2001, 25, 735.
13. Akil, Md.; Cantwell, W. J. Compos B 2002, 33, 193.
14. Abrate, S. Appl Mech Rev 1997, 50, 70.
15. Sanchez-Soto, M.; Martínez, A. B.; Santana, O. O.; Gordillo, A. J Appl Polym Sci 2004, 93, 1271.
16. Chuan-yu, W.; Long-yuan, L.; Thornton, C. Int J Impact Eng 2003, 28, 929.
17. Macaulay, M. A. Introduction to Impact Engineering; Chapman and Hall: London, 1987.
18. Martinez, A. B.; Agulló, J.; Jiménez, O.; Sullcahuamán, J. A.; Sánchez-Soto, M.; Maspoch, M. L. L.; Velasco, J. I.; Santana, O. O.; Gordillo, A. Impacto de baja energía de composites de poliestireno. In: Actas del IV Congreso Nacional de Materiales Compuestos; Bitacora publicidad: Gijon, Spain, 2001; pp 43–78.